applied sciences

MDPI

Article

High Performance of an Adaptive Sliding Mode Controller under Varying Loads for Lifting-Type Autonomous Grounded Robot

Van Ngoc Son Huynh [1,†], Ha Quang Thinh Ngo [1,2,*], Thanh Phuong Nguyen [3] and Hung Nguyen [3]

1 Department of Mechatronics Engineering, Faculty of Mechanical Engineering, Ho Chi Minh City University of Technology (HCMUT), 268 Ly Thuong Kiet Street, District 10, Ho Chi Minh City 700000, Vietnam; 1870060@hcmut.edu.vn

2 Vietnam National University Ho Chi Minh City, Linh Trung Ward, Thu Duc District, Ho Chi Minh City 700000, Vietnam

3 HUTECH Institute of Engineering, Ho Chi Minh City University of Technology (HUTECH), Ho Chi Minh City 700000, Vietnam; nt.phuong@hutech.edu.vn (T.P.N.); n.hung@hutech.edu.vn (H.N.)

* Correspondence: nhqthinh@hcmut.edu.vn

† These authors contributed equally to this work.

Received: 23 June 2020; Accepted: 4 August 2020; Published: 24 August 2020

Abstract: To work in shared space with humans, autonomous systems must carry unknown loads in predefined missions. With the conventional control scheme, the grounded robot would suffer unstable motion and imprecise tracking performance. To overcome these challenges, in this paper, a novel controller using an adaptive sliding mode for autonomous grounded robots (AGR) is proposed. This control strategy takes into consideration uncertain characteristics, varying loads, and external disturbances. To analyze the tracking performance precisely, the overall error of motion system is decoupled into two subsystems where the second-order system is related to the angular tracking error and the third-order system is associated with the linear one. Initially, the dynamics model of the grounded robot is established containing different elements of nonlinear forces in order to address the technical problems. Then, the system state equation of the autonomous system is mentioned to indicate the theoretical characteristics. Based on the proposed controller, the stability of the system is validated by the Lyapunov theorem. From the results of numerical tests, three practical situations consisting of separately linear and circular trajectories with varying loads and an S-curve trajectory of a working map are suggested. The tracking performance validates that the proposed control scheme is, in various scenarios, robust, effective, and feasible. From these superior outcomes, it can be determined obviously the property of our works in accommodating the variations of cargo from applications in distribution centers, material transportation, or handling equipment.

Keywords: control system; sliding mode; Lyapunov; AGR; wheeled robot

1. Introduction

The autonomous grounded robot (AGR) is a kind of mobile robot that can be used in any scenario with prominent applications such as assembly lines, storehouse management, production transportation, or as a part of pick-and-place systems. It appears not only in industry but also in logistics or international trade. The principal motivation of current research is to improve the low rate of AGR applications in reality. This autonomous hardware is expected to be more flexible, modular, and intelligent while it requires less cost for initial installation and uses resources to operate and develop. To solve these drawbacks, numerous developers have studied in a large scale of industrial fields.

In [1,2], a low-cost, efficient vehicle-guiding method using a consumer-grade camera and separated markers was investigated to drive for indoor environments. The symbols of capital letters or triangles which are easy to produce and maintain indicate the routing guide to the target location. In the same directional research, authors [3] applied a multiple-input multiple-output antenna radar to achieve high location precision. The results compared with the traditional global positioning system denoted excellent outcomes for autonomous robots in the port. In the new trend of artificial intelligence, more research related to fuzzy scheme or neural network control has been investigated. To recognize the operating environment and avoid an obstacle intelligently, a fuzzy controller which is constructed by rough sets and an adaptive neuro-fuzzy inference system was presented in [4]. Duration, maximum tracking error, and mean tracking error are computed to clarify the performance. The achievements in saving time and lessening maximum tracking error and mean tracking error have been proven as superior results. In other contexts, due to the complexity of surrounding space and the uncertainty of sensor data, a motion planning system based on hybrid deep learning was addressed [5]. Firstly, the convolutional neural networks to construct an auto-encoder model and reduce the dimension of the input image were initiated. Later, a path-tracking model based on recurrent neural networks was utilized to build the working map. Consequently, a control model and an evaluation model were set. In road environments, it promised highly robust visual navigation and an advanced ability of self-learning for autonomous vehicles.

2. Literature Review

Dynamical reaching method is still the most favorite topic in different engineering applications. They mostly mention the equations of the dynamic system under private form. In the identical format, a kinematic model of a mobile robot can be obtained firstly by system state and input transformation [6]. The saturated state feedback control guaranteed that the special chained form system tended to zero in a finite time. The asymptotic stability was proven by applying the Lyapunov theorem combined with the finite-time control theory. The results have shown that the effectiveness and validity are not only for the chained system, but also for traditional mobile vehicles. Based on the same switching topologies, a multiagent system with second-order separated dynamics addressed the finite-time consensus problem [7]. A distributed protocol was designed to guarantee a finite-time solution for homogeneous agents without predetermined leaders in continuous time domain. The agents asymptotically converged to an average consensus during finite time even though the communication platform among them was varying. In [8,9], with switching topologies, the distributed fixed-time tracking control for high-order uncertain nonlinear multiagent systems was investigated. Under unknown parameters and mismatched disturbances, one follower was assumed to be in serious feedback form. Because of backstepping method and dynamic surface control, this protocol and appropriate adaptive laws were designed lacking information of upper bounds of disturbances.

The important note of the finite-time control technique is that the system state in dynamic features converges to the equilibrium points in a finite time and they remain there. Some benefits of this method are fast rise, short transient time, and high-accuracy performance. To extend their usages, many developers combine the finite-time control with fuzzy control. In [10], the difficulties of adaptive finite-time control for a class of single-input and single-output system were addressed when the nonlinear functions were assumed to be unknown. To overcome these challenges, a backstepping-based adaptive fuzzy finite-time control scheme was proposed. The fuzzy technique was employed to recognize the nonlinear uncertainties. The stable system state was verified by Lyapunov stability theory in finite time. Therefore, most of closed signals are semiglobally practical finite-time stable whilst the tracking error tends to a small neighborhood of stable points. Inspired by prescribed performance control, a novel performance function named finite-time performance function was defined [11]. The integration of neural networks and backstepping technology ensured that tracking error converged to an arbitrarily local region at any settling time. The signals in closed-loop systems

are semiglobally practical finite-time stable. With nonstrict feedback structure, a class of nonlinear systems was confirmed to show superior performance.

The autonomous grounded robot (AGR) is a type of electromechanical device which is favored for operating in complex spaces. The AGR is equipped by automating operation, decision making, and adapting capabilities. In order to upgrade the tracking control performance of the AGR, the nonlinear dynamic techniques are adopted for linearization [12], sliding mode control [13], or smart decision [14]. Recently, an improved linear extended state observer with error compensating term has been mentioned [15]. In reality, the uncertain nonlinear kinematic model still exists. It is hard to compute exactly the nonlinear components to enhance the tracking control. Hence, the total uncertainties of the robot are estimated by switching gains to adapt to parameter variations and external disturbances. The tracking errors converge to the desired values by reason of Lyapunov stability theory. To avoid singularity and retain the benefits of sliding mode control, an adaptive sliding control is done [16]. Dealing with external disturbances and inertia uncertainties, the system state is maintained on sliding surfaces without any constraints. Using Lyapunov theorem, a novel fast nonsingular sliding technique could be validated. In another target control, investigators in [17,18] have implemented an adaptive sliding mode control for offshore container cranes that bring containers from a massive ship to a smaller boat. After decoupling the actuated and unactuated joint variables, a sliding surface that integrated with the decoupled dynamics was designed. The vibration suppression is effective in the presence of ship motion, large swings, unknown parameters, and sudden disturbances.

3. Problem Definition

The scope of this research focuses on tracking control of AGRs that often work in warehouses or distribution centers. The first work was to construct the hardware platform of an advanced AGR [19] to overcome the limitations of present products in the market. The computer-aided design is shown in Figure 1. Unlike the other towing cars, this robot is able to carry cargo by lifting the rack. This useful design supports it in traveling, rapid execution of tasks, and flexible motion. Our research has successfully developed a practical model of an AGR as shown in Figure 2. When it executes in the working map, the technical problems produce low-quality control. In the effort to enhance the system performance, developers in [20] recommended the Lyapunov control for both position and velocity constraints. Unfortunately, the uncertainties did not take into account the dynamic model, hence, it might cause some incorrect results when using real-world hardware. In [21], the vision approach was considered as a control application in assisting the worker to carry heavy loads. The drawbacks of this method are such that it is hard to evaluate the precision tracking mission and its performance mainly depends on the working environment and focal length of the digital camera. The other method is to employ the expert-based knowledge in velocity and positioning control [22]. The decision to drive two wheels derives from heavy levels of cargo and how tracking errors occur. Several disadvantages of the fuzzy logic control approach in AGRs are that it rests on the operator's experiences too much and the stable convergence is not verified yet. Besides, the nonlinear performance still happens because of unknown parameter variations and disturbances. As a result, there is a need to design a novel controller that is adapted to uncertainties. As well, the motion controller must guarantee the stable system state whenever the AGR operates.

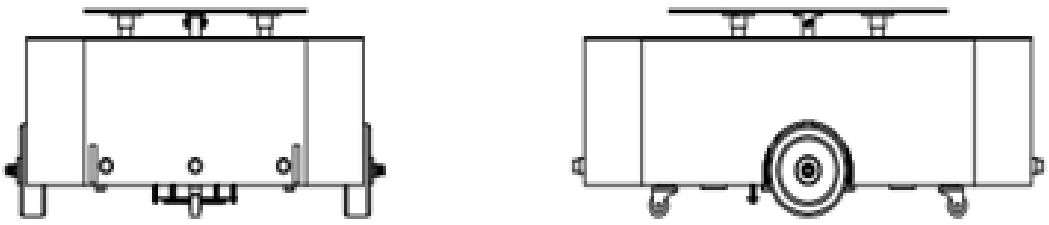

Figure 1. Computer-aided design for autonomous grounded robot (AGR) (**left**: front side of robot, **right**: side view of robot).

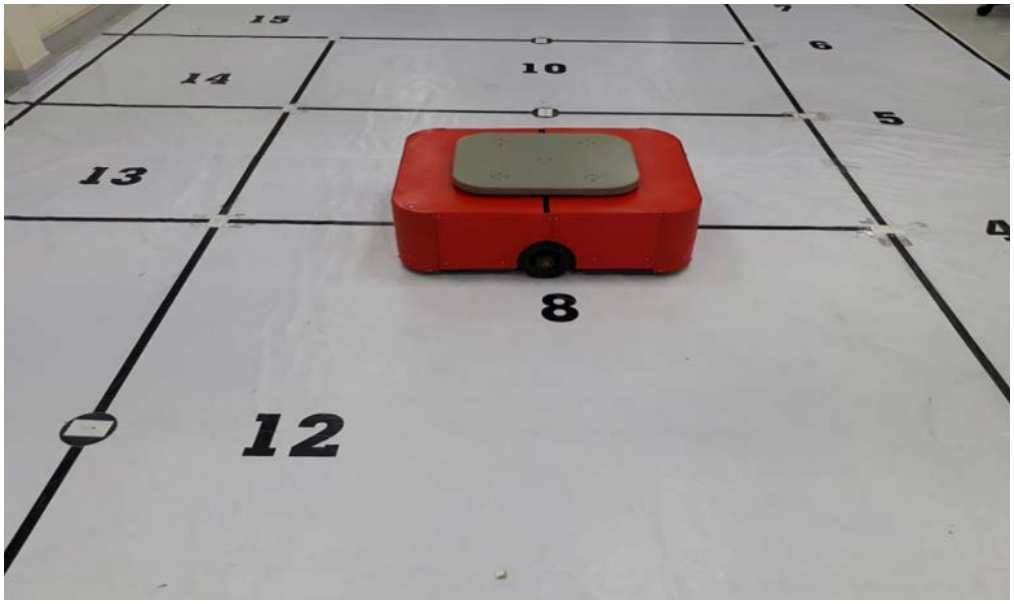

Figure 2. Experimental platform of AGR.

4. Theoretical Works

The specified prototype of the wheeled vehicle is depicted in Figure 3. It belongs to the Differential-Driving-Wheel (DDW) type which is actively driven by two side wheels and set free for two front and back ones. Consider that $2b$, $2r$, θ, and θ_d are the length between two wheels, diameter of wheel, differences between actual, desired heading angle and Ox, respectively. When the mobile vehicle moves on planar ground, there is no variation in Oz. Perfectly, the distribution of the robot's weight is uniform and its central mass is located in the middle of the active driven wheels. We assume that the vector of system state $q^T = \begin{bmatrix} x & y & q \end{bmatrix}$ represents location and driving angle, $\vartheta^T = \begin{bmatrix} v & \omega \end{bmatrix}$ defines the kinematic information.

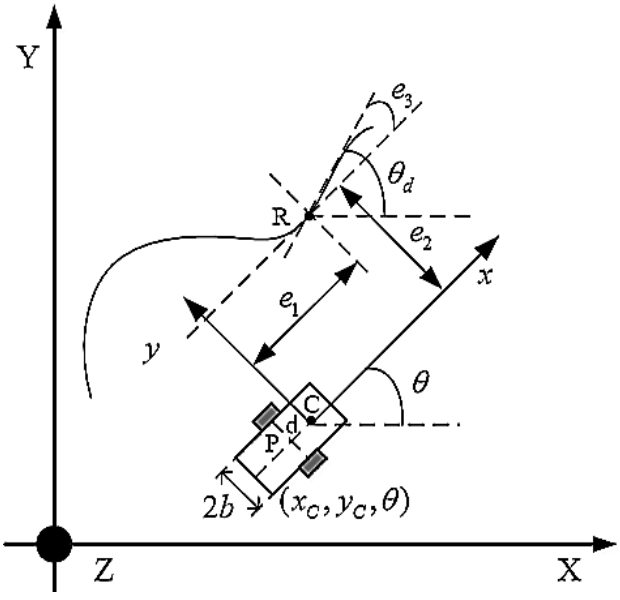

Figure 3. Modeling of wheeled autonomous robot.

The relationship amongst linear velocity and angular velocity with full rank matrix $S(q)$ is expressed as

$$\dot{q} = S(q)\vartheta = \begin{bmatrix} \cos\theta & 0 \\ \sin\theta & 0 \\ 0 & 1 \end{bmatrix} \begin{bmatrix} v \\ \omega \end{bmatrix} \tag{1}$$

A nonholonomic mobile vehicle system having an n-dimensional configuration space C with generalized coordinates ($q1, \ldots, qn$) can be described by:

$$M(q)\ddot{q} + F\left(\dot{q}\right) + \tau_d = B(q)\tau - A^T(q)\lambda \tag{2}$$

where

λ: Lagrange multiplier constraint
$F(\dot{q})$: friction factors
$M(q)$: symmetric and positive-definite inertia matrix
$A(q)$: matrix associated with the constraints
$B(q)$: input transformation matrix
τ_d: disturbances torque
τ_1, τ_2: driving torques of two wheels, $\tau^T = \begin{bmatrix} \tau_1 & \tau_2 \end{bmatrix}$

The Euler–Lagrange equations of motion are used to derive the dynamics of the mobile vehicle systems. The dynamical equations of the mobile vehicle system can be expressed as:

$$M(q) = \begin{bmatrix} m & 0 & 0 \\ 0 & m & 0 \\ 0 & 0 & J \end{bmatrix}, \; B(q) = \frac{1}{r}\begin{bmatrix} \cos\theta & \cos\theta \\ \sin\theta & \sin\theta \\ b & -b \end{bmatrix} A^T(q) = \begin{bmatrix} -\sin\theta \\ \cos\theta \\ 0 \end{bmatrix}$$

where

J: inertia moment
m: total weight of system

Assumption 1: The vehicle system has three-dimensional configuration space with generalized coordinate vector q, subject to nonslipping and pure rolling.

$$A(q)\dot{q} = 0 \tag{3}$$

Assumption 2: $S \in \Re^{2\times 3}$ is a full rank matrix satisfying

$$S^T(q)A^T(q) = 0 \tag{4}$$

Assumption 3: It is assumed that the disturbance vector is unknown but bounded.

$$|\tau_d| \leq \partial \tag{5}$$

Remember that the constraint imposed on ∂ is to ensure that the level of uncertain factors is not so large that the stable state of system can be reversed.

Taking derivative of Equation (1), we have

$$\ddot{q} = S(q)\dot{\vartheta} + \dot{S}(q)\vartheta \tag{6}$$

Substituting Equation (6) into Equation (2)

$$M(q)\left(S(q)\dot{\vartheta} + \dot{S}(q)\vartheta\right) + F\left(\dot{q}\right) + \tau_d = B(q)\tau - A^T(q)\lambda \tag{7}$$

Multiplied by $S^T(q)$ in both right and left side

$$S^T(q)M(q)\left(S(q)\dot{\vartheta}+\dot{S}(q)\vartheta\right)+S^T(q)\left(F\left(\dot{q}\right)+\tau_d\right)=S^T(q)B(q)\tau-S^T(q)A^T(q)\lambda \tag{8}$$

From Assumption 2, it can be

$$S^T(q)A^T(q)=0,\ S^T(q)M(q)\dot{S}(q)=0 \tag{9}$$

The dynamic of mobile system becomes

$$\overline{M}\dot{\vartheta}=\overline{B}\tau+d(t) \tag{10}$$

with

$$\overline{M}=\begin{bmatrix} m & 0 \\ 0 & J \end{bmatrix},\ \overline{B}=\frac{1}{r}\begin{bmatrix} 1 & 1 \\ b & -b \end{bmatrix},\ d(t)=-S^T(q)\left(F\left(\dot{q}\right)+\tau_d\right)$$

As a result, the system state variables are rewritten as

$$\dot{q}=\begin{bmatrix} \dot{x} \\ \dot{y} \\ \dot{\theta} \end{bmatrix}=\begin{bmatrix} v\cos\theta \\ v\sin\theta \\ \omega \end{bmatrix} \tag{11}$$

The relationship among interacting forces can be performed

$$\begin{cases} J\dot{\omega}=u_1+d_1(t) \\ m\dot{v}=u_2+d_2(t) \end{cases} \tag{12}$$

where

$$u=\begin{bmatrix} u_1 \\ u_2 \end{bmatrix}=\frac{1}{r}\begin{bmatrix} \tau_1-\tau_2 \\ \tau_1+\tau_2 \end{bmatrix},\ d(t)=\begin{bmatrix} d_1(t) \\ d_2(t) \end{bmatrix}$$

For physical meaning, $d_i(t)$ denotes external noises or uncertain factors. $u_i(t)$ implies the control signal for two wheels.

To address the tracking control troubles, the reference signal is firstly determined so that system errors converge to zero values in finite time.

$$\dot{q}_r=\begin{bmatrix} \dot{x}_r \\ \dot{y}_r \\ \dot{\theta}_r \end{bmatrix}=\begin{bmatrix} v_r\cos\theta_r \\ v_r\sin\theta_r \\ \omega_r \end{bmatrix} \tag{13}$$

$[x_r(t), y_r(t), \theta_r(t)]^T \in \mathfrak{R}^3$, $[v_r(t), \omega_r(t)]^T \in \mathfrak{R}^2$. Then, the tracking error vector is defined as

$$\overline{e}=\begin{bmatrix} e_x \\ e_y \\ e_\theta \end{bmatrix}=\begin{bmatrix} \cos\theta & \sin\theta & 0 \\ -\sin\theta & \cos\theta & 0 \\ 0 & 0 & 1 \end{bmatrix}\begin{bmatrix} x-x_r \\ y-y_r \\ \theta-\theta_r \end{bmatrix} \tag{14}$$

Hence,

$$\dot{\overline{e}}=\begin{bmatrix} \dot{e}_x \\ \dot{e}_y \\ \dot{e}_\theta \end{bmatrix}=\begin{bmatrix} v-v_r\cos e_\theta+\omega e_y \\ v_r\sin e_\theta-\omega e_x \\ \omega-\omega_r \end{bmatrix} \tag{15}$$

In the real world, some constraints related to hardware platform or physical phenomenon still exist inside the system. With no loss of generality, we give the following assumptions.

Assumption 4: The existing positive gains which are tuned could be the upper bound and lower bound of linear velocity and angular velocity.

$$\omega_r^{lower} \le |\omega_r| \le \omega_r^{upper} \tag{16}$$

$$\left|\dot{\omega}_r\right| \le \dot{\omega}_r^{upper} \tag{17}$$

$$|v_r| \le v_r^{upper} \tag{18}$$

$$\left|\dot{v}_r\right| \le \dot{v}_r^{upper} \tag{19}$$

Although the external disturbances or uncertainties are unknown, its positive upper limitation is always remaining so that $\left|d_i(t)\right| \le d^{upper}$

Obviously, the entire design idea is to categorize into angular control problem and positioning control problem as following. Even though the Multi-Input-Multi-Output (MIMO) controller design can be employed in this situation, a separated solution for second-order subsystem and third-order subsystem assists to lessen a burden computation.

$$\begin{cases} \dot{e}_\theta = \omega - \omega_r \\ J\dot{\omega} = u_1 + d_1(t) \end{cases} \tag{20}$$

$$\begin{cases} \dot{e}_x = v - v_r \cos e_\theta + \omega e_y \\ \dot{e}_y = v_r \sin e_\theta - \omega e_x \\ m\dot{v} = u_2 + d_2(t) \end{cases} \tag{21}$$

The establishment of second-order scheme is primarily proposed with some positive parameters $\varepsilon > 0$, $0 < p < 1$. (Appendix A).

$$s_1 = \dot{e}_\theta + k_1 e_\theta + k_2 \Gamma_{e_\theta} \tag{22}$$

where

$$\Gamma_{e_\theta} = \begin{cases} e_\theta^P & \text{if } (\bar{s}_1 \ne 0 \wedge |e_\theta| \ge \varepsilon) \vee \bar{s}_1 = 0 \\ l_1 e_\theta + l_2 {e_\theta}^2 sign(e_\theta) & \text{if } \bar{s}_1 \ne 0 \wedge |e_\theta| < \varepsilon \end{cases} \tag{23}$$

$$\bar{s}_1 = \dot{e}_\theta + k_1 e_\theta + k_2 e_\theta^P \tag{24}$$

$$l_1 = (2-p)\varepsilon^{p-1} \tag{25}$$

$$l_2 = (p-1)\varepsilon^{p-2} \tag{26}$$

Therefore,

$$J\dot{s}_1 = f_1 + u_1 \tag{27}$$

where

$$f_1 = J\left(k_1 + k_2 \Psi_{e_\theta}\right)\dot{e}_\theta - J\dot{\omega}_r + d_1(t) \tag{28}$$

$$\Psi_{e_\theta} = \begin{cases} p e_\theta^{p-1} & \text{if } (\bar{s}_1 \ne 0 \wedge |e_\theta| \ge \varepsilon) \vee \bar{s}_1 = 0 \\ l_1 + 2 l_2 e_\theta sign(e_\theta) & \text{if } \bar{s}_1 \ne 0 \wedge |e_\theta| < \varepsilon \end{cases} \tag{29}$$

The unknown factor f_1 can be limited as

$$\left|f_1\right| \le J\left|k_1 + k_2 \Psi_{e_\theta}\right|\left|\dot{e}_\theta\right| + J\left|\dot{\omega}_r\right| + \left|d_1(t)\right| \le a_1 + b_1|z_1| \tag{30}$$

a_1, b_1 are some positive values, $|z_1| = \sqrt{\dot{\theta}_e^2 + \theta_e^2}$. Consider that we can write $a_1^2 = \phi_1$, $b_1^2 = \chi_1$, and $\widetilde{\phi}, \widetilde{\chi}$ are the estimators of ϕ, χ, correspondingly. We obtain the related quantity among estimators as

$$\widetilde{\kappa}_1 = \frac{1}{2\varepsilon_1^2}\widetilde{\phi}_1 + \frac{1}{2\varepsilon_2^2}\widetilde{\chi}_1 z_1^2 \tag{31}$$

Thus, the controller for second-order structure is investigated as

$$u_1 = -(\beta_1 + \widetilde{\kappa}_1)s_1 \tag{32}$$

$\beta_1, \varepsilon_1, \varepsilon_2$ are constants and non-negative. The adaptive laws should be selected as

$$\dot{\widetilde{\phi}}_1 = -\varepsilon_1\widetilde{\phi}_1 + \frac{1}{2\varepsilon_1^2}s_1^2 \tag{33}$$

$$\dot{\widetilde{\chi}}_1 = -\varepsilon_2\widetilde{\chi}_1 + \frac{z_1^2}{2\varepsilon_2^2}s_1^2 \tag{34}$$

From here, it yields that

$$J\dot{s}_1 = -\beta_1 s_1 + \widetilde{\Upsilon}_1 \tag{35}$$

where

$$\widetilde{\Upsilon}_1 = f_1 - \widetilde{\kappa}_1 s_1$$

Theorem 1. *With the dynamic expression (35), $s_1, \widetilde{\phi}_1$ and $\widetilde{\chi}_1$are uniformly and ultimately bounded with the adaptive control law (33–34).*

Proof: Select the Lyapunov candidate as

$$V_1 = \frac{1}{2}\left(Js_1^2 + \phi_1^2 + \chi_1^2\right) \tag{36}$$

where

$$\breve{\phi}_1 = \phi_1 - \widetilde{\phi}_1, \breve{\chi}_1 = \chi_1 - \widetilde{\chi}_1$$

The first derivative of V_1

$$\begin{aligned}
\dot{V}_1 &\le -\beta_1 s_1^2 - \widetilde{\kappa}_1 s_1^2 + a_1|s_1| + b_1|z_1||s_1| - \breve{\phi}_1\dot{\widetilde{\phi}} - \breve{\chi}_1\dot{\widetilde{\chi}}_1 \\
&\le -\beta_1 s_1^2 - \widetilde{\kappa}_1 s_1^2 + \frac{\phi_1 s_1^2}{2\varepsilon_1^2} + \frac{\chi_1 s_1^2 z_1^2}{2\varepsilon_2^2} - \frac{(\phi_1 - \widetilde{\phi}_1)s_1^2}{2\varepsilon_1^2} - \frac{(\chi_1 - \widetilde{\chi}_1)s_1^2 z_1^2}{2\varepsilon_2^2} + \varepsilon_1\breve{\phi}_1\widetilde{\phi}_1 + \varepsilon_2\breve{\chi}_1\widetilde{\chi}_1 + \frac{\left(\varepsilon_1^2 + \varepsilon_2^2\right)}{2} \\
&\le -\beta_1 s_1^2 - \varepsilon_1\breve{\phi}_1\left(\breve{\phi}_1 - \phi_1\right) - \varepsilon_2\breve{\chi}_1\left(\breve{\chi}_1 - \chi_1\right) + \frac{\left(\varepsilon_1^2 + \varepsilon_2^2\right)}{2} \\
&\le -\beta_1 s_1^2 - \frac{\sigma_1\breve{\phi}_1^2}{2} - \frac{\sigma_2\breve{\chi}_1^2}{2} + \xi_1 \\
&\le -\alpha_1 V_1 + \xi_1
\end{aligned} \tag{37}$$

where $\sigma_1 = \frac{\varepsilon_1(2l_1-1)}{l_1}$, $\sigma_2 = \frac{\varepsilon_2(2l_2-1)}{l_2}$, $\sigma_3 = \frac{l_1\varepsilon_1}{2}$, $\sigma_4 = \frac{l_2\varepsilon_2}{2}$, $\xi_1 = \frac{\left(\varepsilon_1^2+\varepsilon_2^2\right)}{2} + \sigma_3\phi_1^2 + \sigma_4\chi_1^2$, $\alpha_1 = \left\{\min\left(\sigma_1, \sigma_2, \frac{2\beta_1}{J}\right)\right\}$. Using theorem in [5], whole signals in mobile system (35) are uniformly and ultimately bounded. Consequently, it is proven that $\widetilde{\Upsilon}_1$ is bounded, meaning $\left|\widetilde{\Upsilon}_1\right| \le \Upsilon_1^{upper}$, $\Upsilon_1^{upper} > 0$. □

Remark 1. *To attain the stable state when time reaches any finite instant, the control law should be modified as:*

$$\overline{u}_1 = -(\beta_1 + \widetilde{\kappa}_1)s_1 - \varphi_1 \text{sign}(s_1)|s_1|^{\frac{1}{2}} \tag{38}$$

with $\varphi_1 > 0$. *Substituting Equation (38) into Equation (35)*

$$J\dot{s}_1 = -\beta_1 s_1 + \widetilde{\Upsilon}_1 - \varphi_1 \text{sign}(s_1)|s_1|^{\frac{1}{2}} \tag{39}$$

As the proposed control law (38) guarantees that the tracking angular error converges to the small region in finite time, we could obtain $sin(e_\theta) \to 0$ and $cos(e_\theta) \to 1$. Later, the subsystem (21) can be simplified to

$$\begin{cases} \dot{x}_e = v - v_r + \omega_r y_e \\ \dot{y}_e = -\omega_r x_e \\ m\dot{v} = u_2 + d_2(t) \end{cases} \tag{40}$$

Now, we can elect the transitional variable as $e_\omega = x_e - sign(\omega_r) y_e$ and $\dot{e}_\omega = v - v_r + \omega_r y_e + \left|\omega_r\right| x_e$. Then, a sliding mode surface is constructed as

$$s_2 = \dot{e}_\omega + k_1 e_\omega + k_2 \Gamma_{e_\omega} \tag{41}$$

$$\Gamma_{e_\omega} = \begin{cases} e_\omega^p, \text{ if } (\overline{s_2} \neq 0 \wedge |e_\omega| > \varepsilon) \ \vee \ \overline{s_2} = 0 \\ l_1 e_\omega + l_2 \text{sign}(e_\omega) {e_\omega}^2, \text{ if } \overline{s_2} \neq 0 \wedge \ \text{e}_\omega < \varepsilon \end{cases} \tag{42}$$

$$\bar{s}_2 = \dot{e}_\omega + k_1 e_\omega + k_2 {e_\omega}^p \tag{43}$$

Following, we consider the below subsystem with coordinate mapping.

$$m\dot{s}_2 = f_2 + u_2 \tag{44}$$

$$\begin{aligned} f_2 = -m\dot{v}_r + d_2(t) - {\omega_r}^2 x_e + m(\left|\dot{\omega}_r\right| x_e + \dot{\omega}_r y_e + \left|\omega_r\right|(v - v_r + \omega_r y_e)) \\ + mk_1 \dot{e}_\omega + mk_2 \dot{e}_\omega \Psi_{e_\omega} \end{aligned} \tag{45}$$

with

$$\Psi_{e_\omega} = \begin{cases} p e_\omega^p, \text{ if } (\ \bar{s}_2 \neq 0 \wedge |e_\omega| > \varepsilon \ ) \vee \ \bar{s}_2 = 0 \\ l_1 + 2 l_2 \text{sign}(e_\omega) e_\omega, \text{ if } \bar{s}_1 \neq 0 \wedge |e_\omega| < \varepsilon \end{cases} \tag{46}$$

With the above assumptions, the nonlinear factor f_2 in system (44) can be bounded by

$$\left|f_2\right| \leq m\left|\dot{v}_r\right| + \left|d_2(t)\right| + m\left|\omega_r\right|\left|\dot{\omega}_e\right| + m\left|\dot{\omega}_r\right|\left|\omega_e\right| + m\left|k_1 + k_2 H_{\omega_e}\right|\left|\dot{\omega}_e\right| \leq a_2 + b_2|z_2| \tag{47}$$

where a_2 and b_2 are positive values, $\left|z_2\right| = \sqrt{\dot{e}_\omega^2 + e_\omega^2}$

Lastly, a sliding mode control law is suggested as

$$u_2 = -(\beta_2 + \hat{\kappa}_2) s_2 \tag{48}$$

where a_2, b_2 are positively tuning gains. Consider that $a_2^2 = \phi_2$, $b_2^2 = \chi_2$. $\widetilde{\phi}, \widetilde{\chi}$ are the estimators of ϕ, χ, respectively, thus the relationship among estimators is

$$\hat{\kappa}_2 = \frac{1}{2\varepsilon_3^2} \hat{\phi}_2 + \frac{1}{2\varepsilon_4^2} \hat{\chi}_2 {z_2}^2 \tag{49}$$

The adaptive laws are designed as follows.

$$\dot{\widetilde{\phi}}_2 = -\varepsilon_3 \widetilde{\phi}_2 + \frac{1}{2\varepsilon_3^2} s_2^2 \tag{50}$$

$$\dot{\widetilde{\chi}}_2 = -\varepsilon_4 \widetilde{\chi}_2 + \frac{z_2^2}{2\varepsilon_4^2} s_2^2 \tag{51}$$

ε_3, ε_4 are positive gains. Substituting the sliding mode control law (48) into system (44) yields

$$m\dot{s}_2 = -\beta_2 s_2 + \widetilde{\Upsilon}_2 \tag{52}$$

where

$$\widetilde{\Upsilon}_2 = f_2 - \hat{\kappa}_2 s_2.$$

Theorem 2. *Considering the system in (57), s_2, $\hat{\phi}_2$, $\hat{\chi}_2$ are uniformly and ultimately bounded with the adaptive control law (50–51).*

Proof: Select the Lyapunov function as

$$V_2 = \frac{1}{2}(m{s_2}^2 + \widetilde{\phi}_2^2 + \widetilde{\chi}_2^2) \tag{53}$$

where $\widetilde{\phi}_2 = \phi_2 - \hat{\phi}_2$ and $\widetilde{\chi}_2 = \chi_2 - \hat{\chi}_2$.

Computing the first derivative of V_2, we obtain

$$\dot{V}_2 \leq -(\beta_2 s_2^2 + \hat{\kappa}_2 s_2^2) + a_2|s_2| + b_2|s_2||z_2| - \widetilde{\phi}_2\dot{\hat{\phi}}_2 - \widetilde{\chi}_2\dot{\hat{\chi}}_2 \tag{54}$$

$$\begin{aligned}\dot{V}_2 \leq\ & -\beta_2 s_2^2 - \hat{\kappa}_2 s_2^2 + \tfrac{\phi_2}{2\varepsilon_3^2} s_2^2 + \tfrac{\chi_2}{2\varepsilon_4^2} z_2^2 s_2^2 - (\phi_2 - \hat{\phi}_2)\tfrac{1}{2\varepsilon_3^2} s_2^2 \\ & -(\chi_2 - \hat{\chi}_2)\ \tfrac{1}{2\varepsilon_4^2} z_2{}^2 s_2^2 + \varepsilon_3\widetilde{\phi}_2\hat{\phi}_2 + \varepsilon_4\widetilde{\chi}_2\hat{\chi}_2 + \tfrac{1}{2}\ (\varepsilon_3^2 + \varepsilon_4^2) \\ \leq\ & -\beta_2 s_2^2 - \tfrac{\sigma_5}{2}\widetilde{\phi}_2^2 - \tfrac{\sigma_6}{2}\widetilde{\chi}_2^2\ + \xi_3 \\ \leq\ & -\alpha_3 V_3 + \xi_3\end{aligned} \tag{55}$$

where $\alpha_3 = min\left\{\sigma_5, \sigma_6, \frac{2\beta_2}{m}\right\}$, $\xi_3 = \frac{1}{2}(\varepsilon_1^2 + \varepsilon_2^2)\ + \sigma_7\phi_1^2 + \sigma_8\chi_1^2$, with $\sigma_5 = \frac{\varepsilon_3(2\tau_3 - 1)}{\tau_3}$, $\sigma_6 = \frac{\varepsilon_4(2\tau_4 - 1)}{\tau_4}$, $\sigma_7 = \frac{\varepsilon_3\tau_3}{2}$, $\sigma_8 = \frac{\varepsilon_4\tau_4}{2}$, $\tau_i > \frac{1}{2}$,$i = 3, 4$. Using the theorem in [5], whole signals in mobile system (52) are uniformly and ultimately bounded. Consequently, it is proven that $\widetilde{\ }_2$ is bounded, meaning $\widetilde{\ }_2| \leq {}_2^{upper}$, ${}_2^{upper} > 0$. □

Remark 2. *The control law is written under compact expression*

$$\overline{u}_2 = -(\beta_2 + \hat{\kappa}_2)s_2 - \varphi_2 sign(s_2)\left|s_2\right|^{\frac{1}{2}} \tag{56}$$

with $\varphi_2 > 0$. Substituting (55) into (52)

$$m\dot{s}_2 = -\beta_2 s_2 + \widetilde{\ }_2 - \varphi_2 sign(s_2)\left|s_2\right|^{\frac{1}{2}} \tag{57}$$

As the proposed control law (55) guarantees that the tracking angular velocity error converges to the small region in finite time, we could obtain $sin(e_\omega) \to 0$ *and* $cos(e_\omega) \to 1$.

5. Results of Research

Generally, to certify the correctness and fitness of our approach, a series of numerical simulation tests, such as tracking circular reference path, linear trajectory under varying loads, and S-curve shape of working space, has been completed in this section. According to previous research, our model has been built with physical parameters as in Table 1. In the computer's environment, the design was modified so that each computational time did not have much cost and step sizes were all set to 0,1. We considered that the initial reference location of the AGR was $(x_r(0), y_r(0), \theta_r(0)) = (2, 1, 0.25\pi)$. In

addition, the reference linear velocity and angular velocity were $v_r = 3\,m/s, \omega_r = 1.5\,rad/s$. At the beginning, the AGR stayed at $(x(0), y(0), \theta(0)) = (3, 0, 0.4)$.

Table 1. List of system parameters for AGR.

Parameter	Value	Unit
b	0.5	m
r	0.2	m
J	4	kg·m^2
m	5	kg
d_1	$0.3\dot{v} + 0.2v + \omega + \cos t.e^{-t}$	
d_2	$0.28\dot{\omega} + v + 0.3\omega + \sin t$	

To handle the numerical simulations, the parameters of the designed controllers were chosen as in Table 2. The adaptive laws were expected to drive the system state to counteract the nonlinear actions. Also, the conditions of asymptotic stability could be achieved when these parameters were respected to guarantee. To visualize the adaptation, two circumstances were suggested such that the mass of the vehicle was 23 kg with respect to a nonloading case and the total mass of the vehicle was 73 kg corresponding to a full-load case. The tracking performance of circular trajectory and velocities are shown in Figures 4 and 5, respectively. The circular reference path was assumed for the AGR to follow and there was no extreme variation in system state when loads changed. Although the speeds differed basically in the initial stage, it tended to the desired value in a short time. Figure 6 indicates the following errors in (x, y) and θ for tracking circular path. Regarding the effect of the proposed controller, it is clear that the tracking errors including e_x, e_y, e_θ converged to a small region nearly equal to zero in finite time. In this case, convergence time was 1.5 s, which depended on the initial position and orientation of the mobile robot and the parameters.

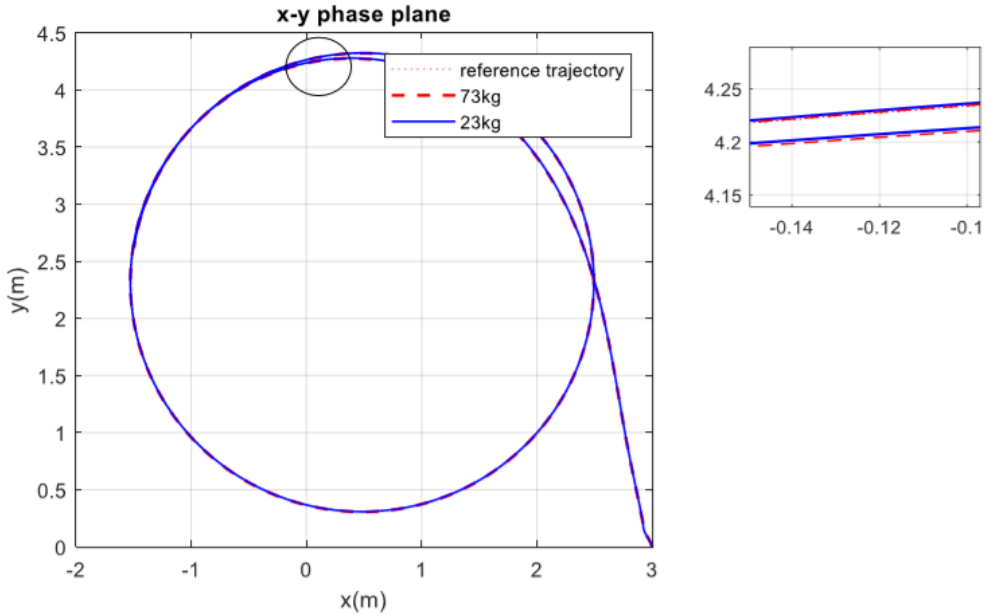

Figure 4. Result of tracking circular trajectory under varying loads.

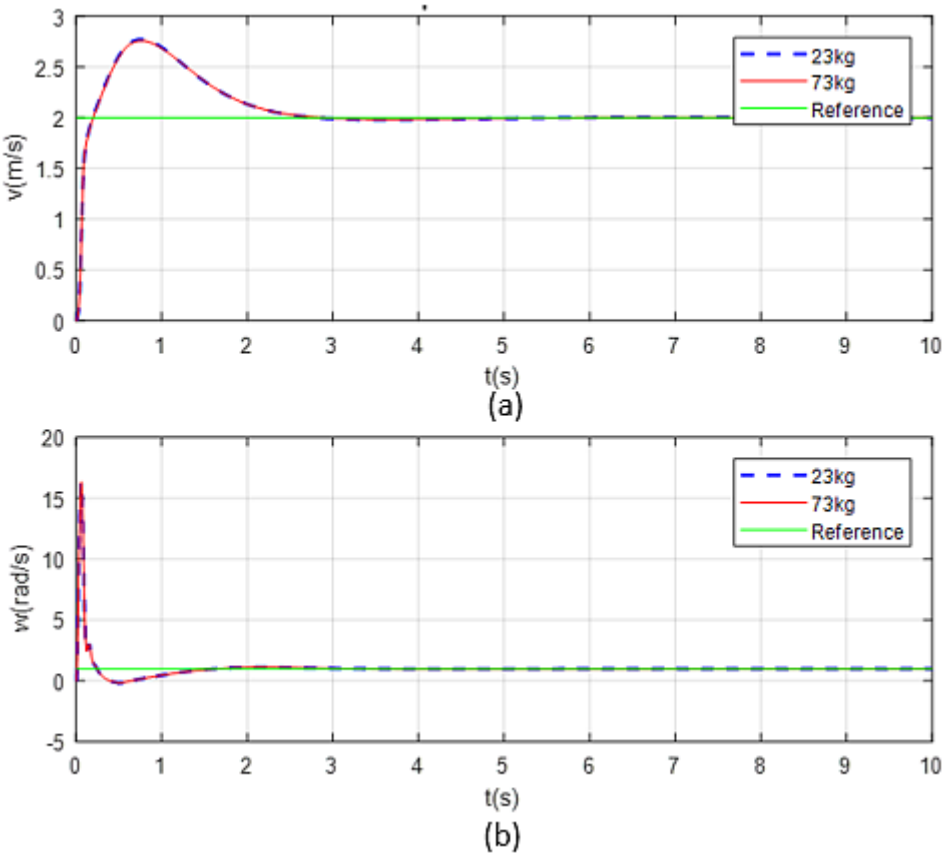

Figure 5. Result of linear velocity (**a**) and angular velocity (**b**) in tracking circular trajectory under varying loads.

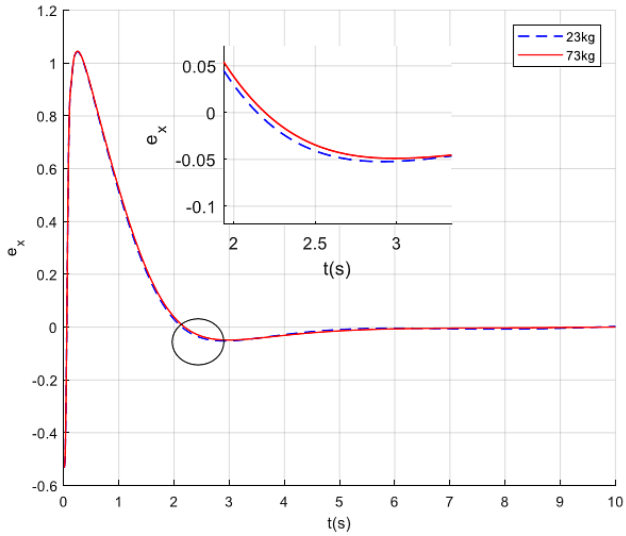

(**a**)

Figure 6. *Cont.*

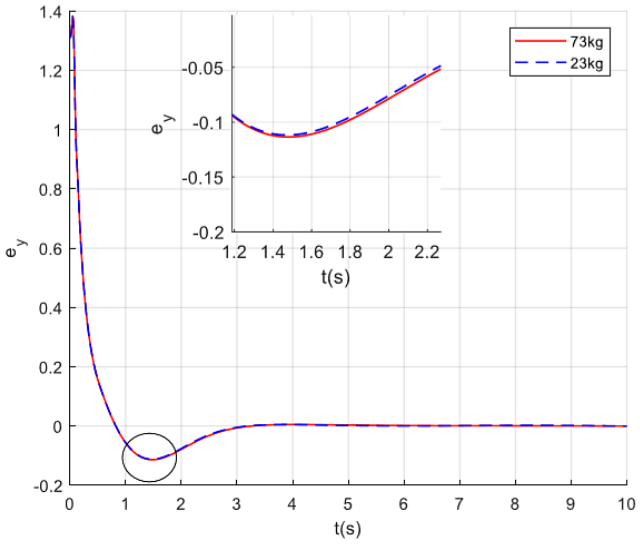

(**b**)

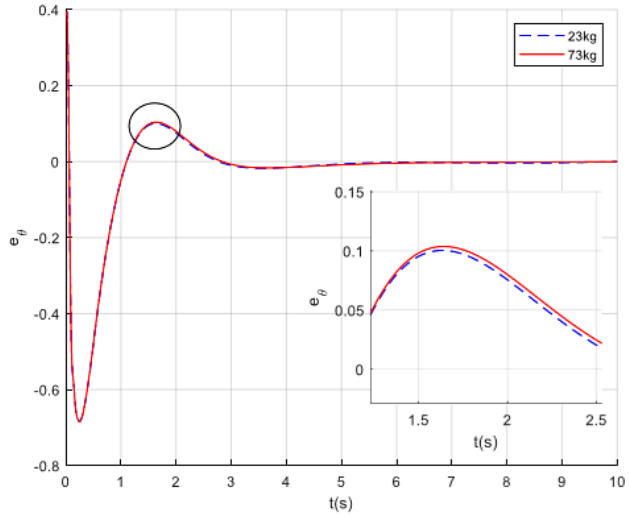

(**c**)

Figure 6. Result of linear errors e_x (**a**), e_y (**b**), and angular error e_θ (**c**) in tracking circular trajectory under varying loads.

Table 2. List of tuning parameters for AGR controller.

Parameter	Value	Parameter	Value
$\beta_1 = \beta_2$	70	k_1	15
$\varepsilon_1 = \varepsilon_3$	5	k_2	3
$\varepsilon_2 = \varepsilon_4$	3	ε	0.005
$\sigma_1 = \sigma_2$	15	$\widetilde{\phi}_1(0)$	0.1
p	$\frac{5}{7}$	$\widetilde{\chi}_1(0)$	0.2
$\widetilde{\phi}_2(0)$	0.3	$\widetilde{\chi}_2(0)$	0.15

In the effort to reveal the advantages of our approach, the tracking performance in a linear reference path under load variations is shown in Figure 7. Additionally, the test information including linear velocity and circular velocity is noticed in Figure 8. In a straight line trajectory, the autonomous robot seemed, with no trouble, to track the desired velocity in any situation. The output tracking resulted in errors under various loads as depicted in Figure 9. In a short time, the adaptation of the

proposed scheme impacted on system state to drive to reduce the differences in the two axes (x, y) and θ. It is admitted that the output results were reasonable while the convergence time was still ensured.

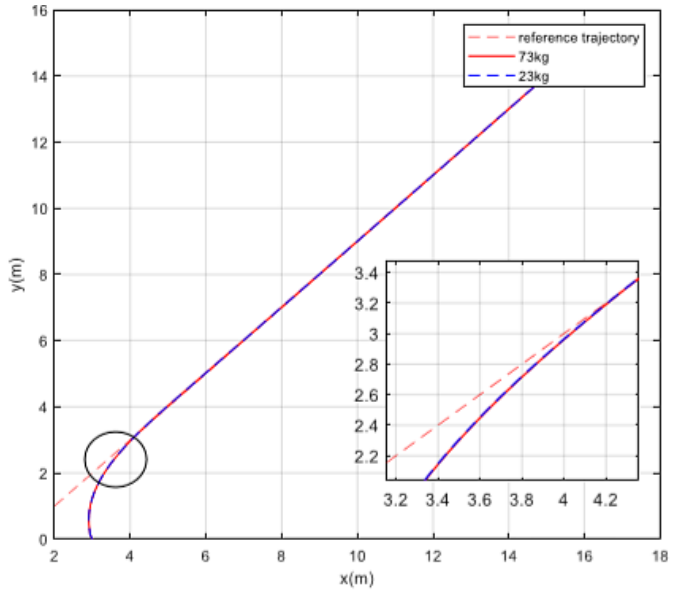

Figure 7. Result of tracking linear trajectory under varying loads.

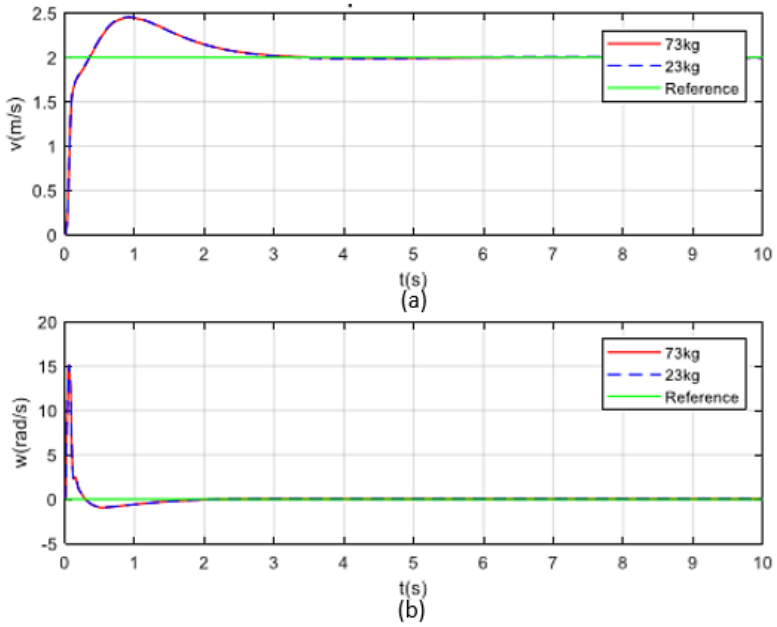

Figure 8. Result of linear velocity (**a**) and angular velocity (**b**) in tracking linear trajectory under varying loads.

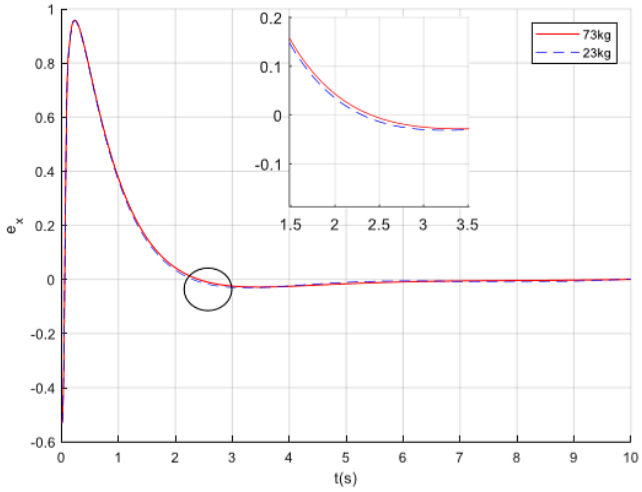

(**a**)

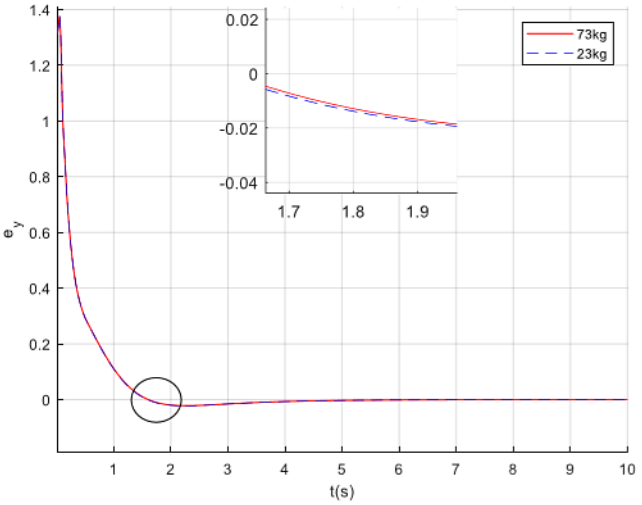

(**b**)

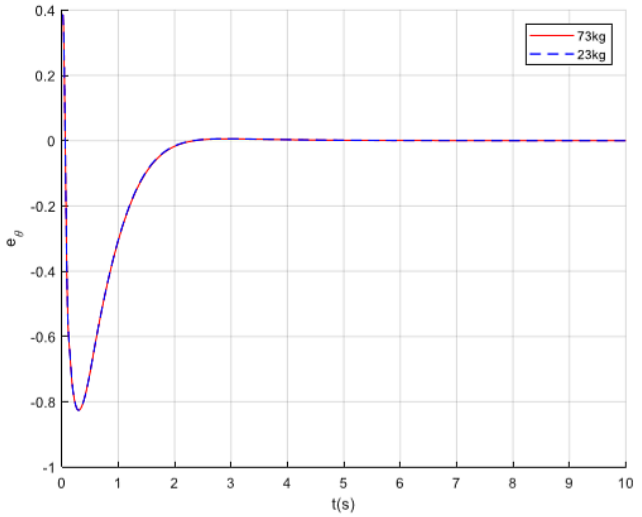

(**c**)

Figure 9. Result of linear errors e_x (**a**), e_y (**b**), and angular error e_θ (**c**) in tracking linear trajectory under varying loads.

More specifically, the real S-curve of the working map as in Figure 10a is suggested for the AGR to confirm the robustness and correctness of the proposed algorithm. For continuous trajectories as in Figure 10b, the robot must follow the alterations of the reference path and decide to drive the whole system immediately. In this test, the tracking performance in the circle path was not as good as the one in the line path. It can be explained that the AGR changed both linear and angular velocity as in Figure 11 to adapt with the unexpected fluctuations in trajectory when it entered a corner.

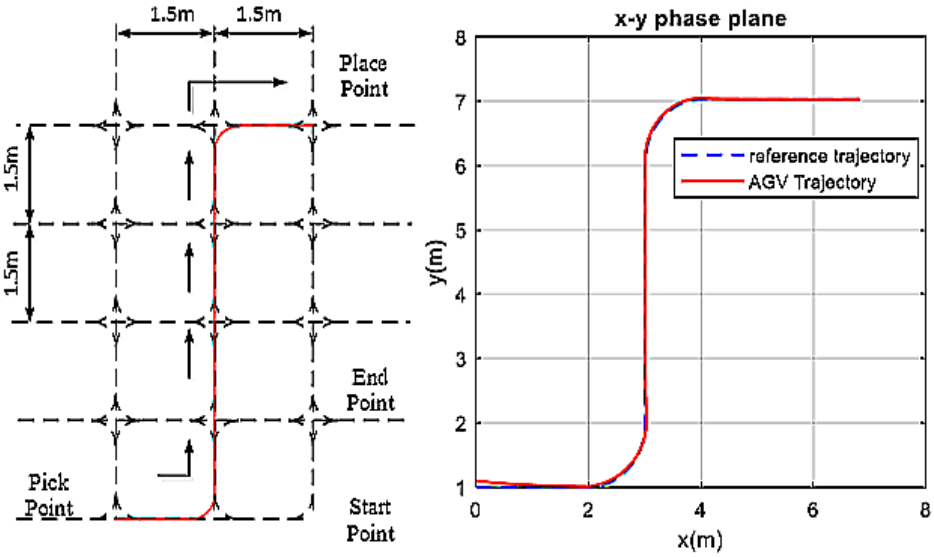

Figure 10. Real S-curve of working map (**a**) and tracking result with continuous linear and circular trajectory (**b**).

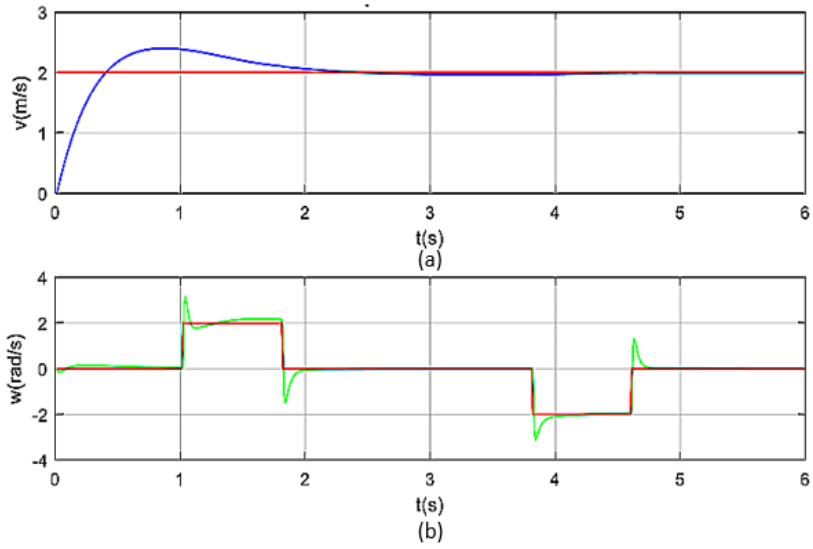

Figure 11. Performance of linear velocity (**a**) and angular velocity (**b**) in tracking S-curve of working map.

In detail, the tracking errors in linear direction and angular movement for the S-curve reference path are demonstrated in Figure 12. The errors still existed in tracking the desired map when the robot executed its task in the warehouse. Under the effective driving of the proposed controller, the existing errors tended to zero in finite time.

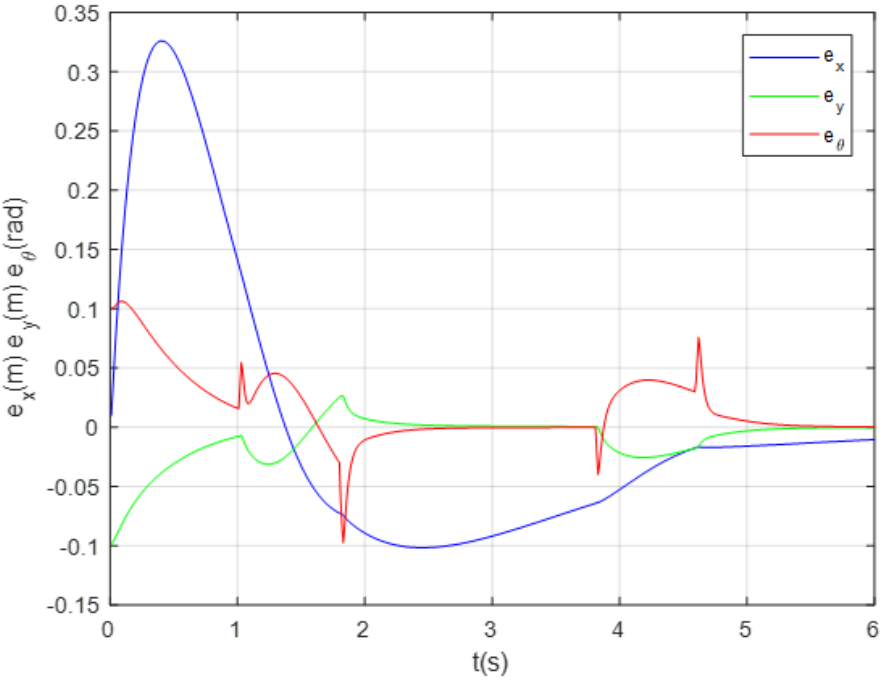

Figure 12. Performance of linear errors e_x, e_y and angular error e_θ in tracking S-curve of working map.

Competitive performance of tracking trajectory for the autonomous robot should be required. Typical robust nonlinear control (TRNC) [23] was chosen since it is popular and proper for industrial applications. In the same context, both robust nonlinear controller and proposed controller must drive the robot model to trace the desired path as in Figure 13. It can be seen clearly that the robust nonlinear scheme early tracked the reference line by tuning the appropriate gains. Our controller needed a finite moment to follow for the reason of the complicated process of the mathematical algorithm. Reversely, the proposed scheme reveals the strong effect to stabilize the autonomous system and reduce the tracking error significantly. With robust nonlinear control, larger uncertainties and small velocity/acceleration could cause the unstable system state. As a result, the tracking errors in this case were still enormous.

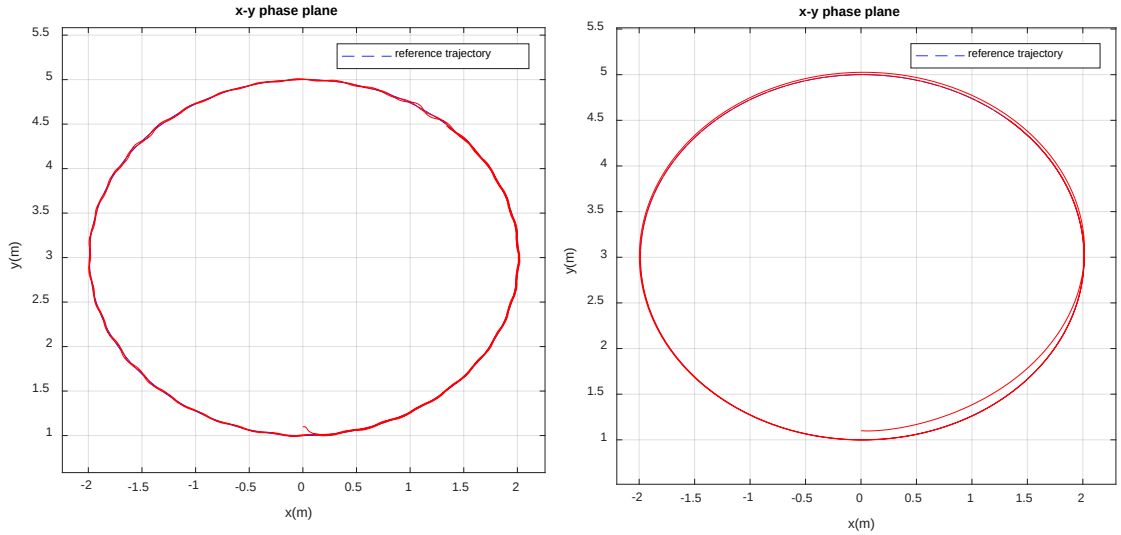

(**a**) (**b**)

Figure 13. Tracking performance of circular trajectory by Typical robust nonlinear control (TRNC) (**a**) and proposed controller (**b**).

Thereafter, the comparative parameters between TRNC and proposed control are linear velocity and angular velocity individually as in Figure 14. During the whole process, the variations in load affected the velocity performance of TRNC. Although it suffered the unknown uncertainties, the proposed control strategy for grounded robot carried out the driving command perfectly. In a short period, the velocity performance of our controller did not possess the changes suddenly and continuously. It is also important to note that the terms of tracking errors are always the crucial factors in order to discover the superior response. Obviously, in Figure 15, the considerable oscillations in both linear and angular velocity are reminders that there exist several disadvantages of TRNC. The adaptive rule might enhance our controller to overcome the varying loads.

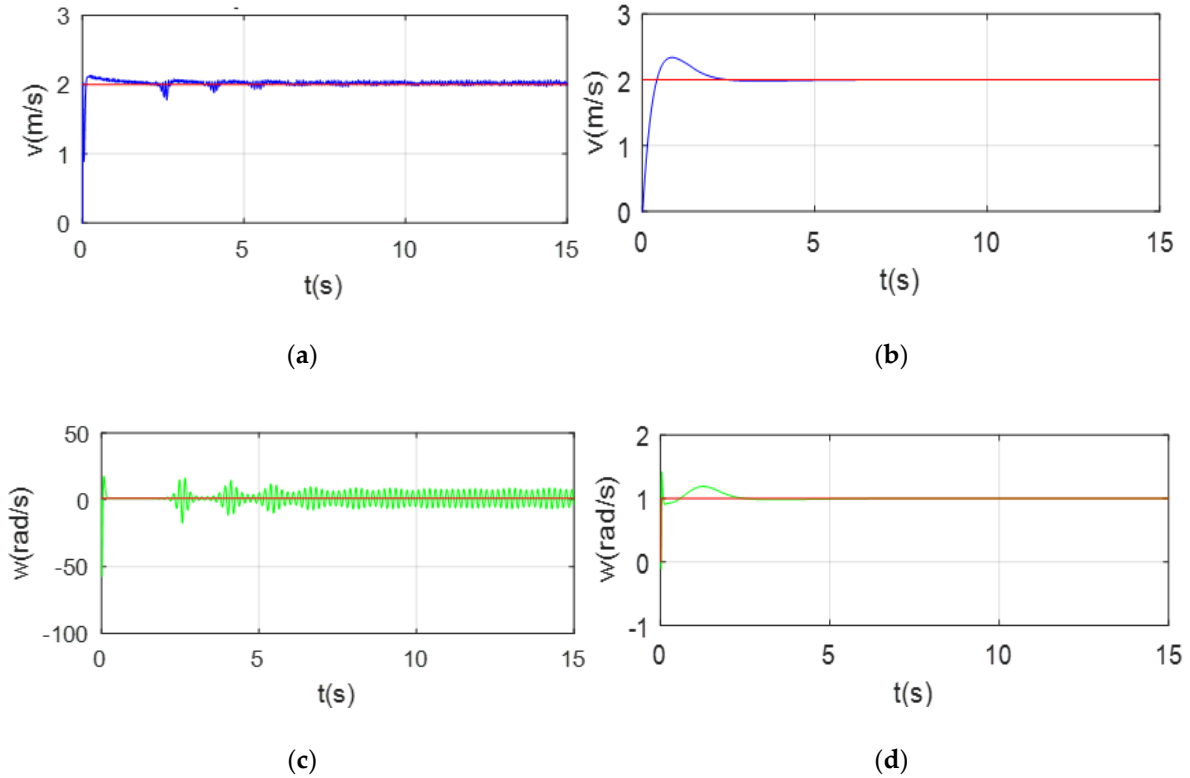

Figure 14. Performance of linear velocity by TRNC (**a**) and proposed controller (**b**); angular velocity by TRNC (**c**) and proposed controller (**d**).

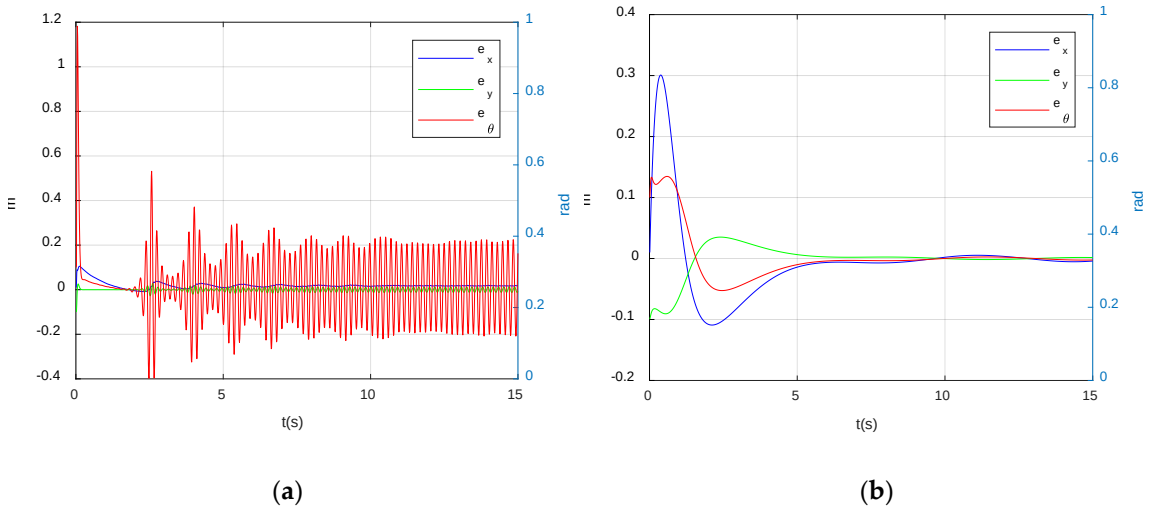

Figure 15. Performance of tracking errors by TRNC (**a**) and proposed controller (**b**).

Table 3 describes the different results of the proposed scheme and TRNC in tracking errors. To provide all views of system performance, three kinds of values (maximum, minimum, and root mean square) are listed. From these results, it could be concluded that TRNC could not reach the stability along the overall trajectory while our approach did well.

Table 3. Comparative results between two controllers (max, min, and root mean square (RMS) value of tracking errors).

	Tracking Error	Max	Min	RMS
Proposed Controller	e_x (m)	0.106	−0.017	0.068
	e_y (m)	0.035	−0.1	0.016
	e_θ (rad)	0.134	−0.053	0.078
TRNC	e_x (m)	0.17	−0.049	0.082
	e_y (m)	0.106	−0.012	0.035
	e_θ (m)	0.18	−0.054	0.103

6. Conclusions

In this paper, a novel adaptive sliding mode controller for AGRs in the field of logistics has been mentioned. In the presence of external disturbance and uncertain inertia, the whole control system is bound to fluctuate. From the analysis of modeling, the dynamic characteristics of the AGR have been classified into subsystems. To reveal the efficacy, two subcontrollers have been introduced to adopt the system variations. Both of them were proven to achieve the asymptotic stability via Lyapunov theorem. Then, a systematic verification including various test cases ensured the proposed design met our requirements. In initial validation, the tracking performance was suggested in linear trajectory and curvable path separately. Later, a complex map mixing linear and circular line was employed to obtain the system response. From the superior simulation results, it was obviously seen that our approach is effective, feasible, and applicable for numerous industrial applications.

The contribution of this article is outlined below. Firstly, the practical problem in lifting-type autonomous robots has been addressed. We were responsible for dominating the characterized platform of mobile robots in order to integrate the theoretical algorithm actively. Secondly, a vehicle-like model was established in the computer environment with the same system configuration. Thirdly, an adaptive sliding mode controller was investigated to drive the autonomous grounded robot under varying loads. It was proven that system stability could be achieved in finite time and tracking performance is greater.

Author Contributions: Conceptualization, V.N.S.H. and H.Q.T.N.; methodology, H.Q.T.N.; software, V.N.S.H.; validation, T.P.N.; formal analysis, H.N.; investigation, V.N.S.H.; resources, T.P.N.; data curation, H.N.; writing—original draft preparation, H.Q.T.N.; writing—review and editing, H.Q.T.N.; visualization, V.N.S.H.; supervision, T.P.N.; project administration, H.N.; funding acquisition, T.P.N. All authors have read and agreed to the published version of the manuscript.

Funding: This research received no external funding.

Acknowledgments: This research is funded by Ho Chi Minh City University of Technology (HCMUT), VNU-HCM, under grant number BK-SDH-2020-1870060. We acknowledge the support of time and facilities from Ho Chi Minh City University of Technology (HCMUT), VNU-HCM for this study.

Conflicts of Interest: The authors declare no conflict of interest.

Appendix A

Regarding $\varepsilon > 0$ and $0 < p < 1$, l_1, l_2 are defined in (25) and (26), correspondingly. With $\beta_1 > 0$, in order to ensure $\alpha_1 > 0$, σ_1 and σ_2 must be positive.

Proof: For the case of σ_1, we can obtain:

$$\sigma_1 = \frac{\varepsilon_1(2l_1 - 1)}{l_1} > 0 \tag{A1}$$

$$\Leftrightarrow \frac{(2l_1 - 1)}{l_1} > 0 \tag{A2}$$

$$\Leftrightarrow \begin{bmatrix} \begin{cases} 2l_1 - 1 > 0 \\ l_1 > 0 \end{cases} \\ \begin{cases} 2l_1 - 1 < 0 \\ l_1 < 0 \end{cases} \end{bmatrix}, l_1 \neq 0 \tag{A3}$$

$$\Leftrightarrow \begin{bmatrix} l_1 > \frac{1}{2} \\ l_1 < 0 \end{bmatrix} \tag{A4}$$

From (25), we have

$$(2 - p)\varepsilon^{p-1} > \frac{1}{2} \tag{A5}$$

$$(2 - p)\varepsilon^{p-1} < 0 \tag{A6}$$

It can be seen that (A6) is not satisfied. With $\varepsilon > 0$ and $0 < p < 1$, to ensure that $\sigma_1 > 0$ then,

$$2(2 - p)\varepsilon^{p-1} > 1 \tag{A7}$$

$$\Leftrightarrow 4\varepsilon^{p-1} > 2(2 - p)\varepsilon^{p-1} > 2\varepsilon^{p-1} > 1 \tag{A8}$$

$$\Leftrightarrow \varepsilon^{p-1} > \frac{1}{2} \tag{A9}$$

For the case of σ_2,

$$\sigma_1 = \frac{\varepsilon_1(2l_1 - 1)}{l_1} > 0 \tag{A10}$$

$$\Leftrightarrow \frac{(2l_1 - 1)}{l_1} > 0 \tag{A11}$$

$$\Leftrightarrow \begin{bmatrix} \begin{cases} 2l_1 - 1 > 0 \\ l_1 > 0 \end{cases} \\ \begin{cases} 2l_1 - 1 < 0 \\ l_1 < 0 \end{cases} \end{bmatrix}, l_1 \neq 0 \tag{A12}$$

$$\Leftrightarrow \begin{bmatrix} l_1 > \frac{1}{2} \\ l_1 < 0 \end{bmatrix} \tag{A13}$$

From (26), it can be computed as

$$\begin{bmatrix} (p - 1)\varepsilon^{p-2} > \frac{1}{2} \\ (p - 1)\varepsilon^{p-2} < 0 \end{bmatrix} \Leftrightarrow \begin{bmatrix} 2(p - 1)\varepsilon^{p-2} > 1 \\ \varepsilon^{p-2} > 0 \end{bmatrix} \tag{A14}$$

With $\varepsilon > 0$ and $0 < p < 1$,

$$0 < p < 1 \tag{A15}$$

$$\Leftrightarrow -2 < 2(p - 1) < 0 \tag{A16}$$

$$\Leftrightarrow -2\varepsilon^{p-2} < 2(p - 1)\varepsilon^{p-2} < 0 \tag{A17}$$

To ensure that $\sigma_2 > 0$,

$$\varepsilon^{p-2} > 0 \tag{A18}$$

From (A9) and (A18), by choosing ε in order to meet $\varepsilon^{p-1} > \frac{1}{2}$, σ_1, σ_2 will be larger than 0. □

References

1. Stetter, R.; Witczak, M.; Pazera, M. Virtual diagnostic sensors design for an automated guided vehicle. *Appl. Sci.* **2018**, *8*, 702. [CrossRef]
2. Lee, J.; Hyun, C.H.; Park, M. A vision-based automated guided vehicle system with marker recognition for indoor use. *Sensors* **2013**, *13*, 10052–10073. [CrossRef] [PubMed]
3. Chen, Z.; He, X.; Cao, Z.; Jin, Y.; Li, J. Position estimation of automatic-guided vehicle based on MIMO antenna array. *Electronics* **2018**, *7*, 193. [CrossRef]
4. Xue, H.; Zhang, Z.; Wu, M.; Chen, P. Fuzzy controller for autonomous vehicle based on rough sets. *IEEE Access* **2019**, *7*, 147350–147361. [CrossRef]
5. Shi, C.; Lan, X.; Wang, Y. Motion planning for unmanned vehicle based on hybrid deep learning. In Proceedings of the 2017 International Conference on Security, Pattern Analysis, and Cybernetics (SPAC), Shenzhen, China, 15–17 December 2017; pp. 473–478.
6. Chen, H.; Li, B.; Zhang, B.; Zhang, L. Global finite-time partial stabilization for a class of nonholonomic mobile robots subject to input saturation. *Int. J. Adv. Robot. Syst.* **2015**, *12*, 159. [CrossRef]
7. Wang, F.; Chen, X.; He, Y.; Wu, M. Finite-time consensus problem for second-order multi-agent systems under switching topologies. *Asian J. Control* **2017**, *19*, 1756–1766. [CrossRef]
8. Ning, B.; Zuo, Z.; Jin, J.; Zheng, J. Distributed fixed-time coordinated tracking for nonlinear multi-agent systems under directed graphs. *Asian J. Control* **2018**, *20*, 646–658. [CrossRef]
9. Zhang, D.; Duan, G. Distributed fixed-time consensus tracking for high-order uncertain non-linear multi-agent systems with switching topologies. *IET Control Theory Appl.* **2019**, *13*, 1761–1772. [CrossRef]
10. Wang, H.; Chen, B.; Lin, C.; Sun, Y.; Wang, F. Adaptive finite-time control for a class of uncertain high-order non-linear systems based on fuzzy approximation. *IET Control Theory Appl.* **2017**, *11*, 677–684. [CrossRef]
11. Liu, Y.; Liu, X.; Jing, Y. Adaptive neural networks finite-time tracking control for non-strict feedback systems via prescribed performance. *Inf. Sci.* **2018**, *468*, 29–46. [CrossRef]
12. Kim, D.H.; Oh, J.H. Tracking control of a two-wheeled mobile robot using input-output linearization. *Control Eng. Pract.* **1999**, *7*, 369–374. [CrossRef]
13. Chen, C.Y.; Li, T.H.S.; Yeh, Y.C.; Chang, C.C. Design and implementation of an adaptive sliding-mode dynamic controller for wheeled mobile robots. *Mechatronics* **2009**, *19*, 156–166. [CrossRef]
14. Ranjbarsahraei, B.; Roopaei, M.; Khosravi, S. Adaptive fuzzy formation control for a swarm of nonholonomic differentially driven vehicles. *Nonlinear Dyn.* **2012**, *67*, 2747–2757. [CrossRef]
15. Cui, M.; Liu, W.; Liu, H.; Jiang, H.; Wang, Z. Extended state observer-based adaptive sliding mode control of differential-driving mobile robot with uncertainties. *Nonlinear Dyn.* **2016**, *83*, 667–683. [CrossRef]
16. Zhai, J.Y.; Song, Z.B. Adaptive sliding mode trajectory tracking control for wheeled mobile robots. *Int. J. Control* **2019**, *92*, 2255–2262. [CrossRef]
17. Kim, G.H.; Hong, K.S. Adaptive sliding mode control of an offshore container crane with unknown disturbances. *IEEE/ASME Trans. Mechatron.* **2019**, *24*, 2850–2861. [CrossRef]
18. Loria, A.; Dasdemir, J.; Jarquin, N.A. Leader–follower formation and tracking control of mobile robots along straight paths. *IEEE Trans. Control Syst. Technol.* **2015**, *24*, 727–732. [CrossRef]
19. Ngo, H.Q.T.; Phan, M.H. Design of an open platform for multi-disciplinary approach in project-based learning of an EPICS class. *Electronics* **2019**, *8*, 200. [CrossRef]
20. Truong, Q.T.; Ngo, H.Q.T.; Nguyen, T.P.; Nguyen, H.; Kim, W.H. A novel infrastructure design of industrial autonomous system. *Int. J. Fuzzy Log. Intell. Syst.* **2019**, *19*, 103–111. [CrossRef]
21. Tran, H.A.M.; Ngo, H.Q.T.; Nguyen, T.P.; Nguyen, H. Implementation of vision-based autonomous mobile platform to control by A∗ algorithm. In Proceedings of the 2018 2nd IEEE International Conference on Recent Advances in Signal Processing, Telecommunications & Computing (SigTelCom), Ho Chi Minh City, Vietnam, 29–31 January 2018; pp. 39–44.

22. Ngo, H.Q.T.; Tran, A.S. Using fuzzy logic scheme for automated guided vehicle to track following path under various load. In Proceedings of the 2018 4th IEEE International Conference on Green Technology and Sustainable Development (GTSD), Ho Chi Minh City, Vietnam, 23–24 November 2018; pp. 312–316.
23. Kanayama, Y.; Kimura, Y.; Miyazaki, F.; Noguchi, T. A stable tracking control method for an autonomous mobile robot. In Proceedings of the IEEE International Conference on Robotics and Automation, Cincinnati, OH, USA, 13–18 May 1990; pp. 384–389.